Batteries & Supercaps

Research Article
doi.org/10.1002/batt.202500348

Chemistry Europe
European Chemical Societies Publishing

www.batteries-supercaps.org

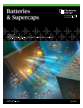

Enhanced Reversibility of Mg Plating/Stripping via Solvation Sheath Regulation by a Multidentate Linear Oligoether

Toshihiko Mandai

Magnesium (Mg) is an abundant resource, and rechargeable Mg metal batteries (RMMBs) could help to achieve a sustainable society. However, practical Mg batteries require electrolyte materials compatible with both positive and negative Mg metal electrodes. Weakly coordinating anion (WCA)-based electrolytes meet these requirements and have had a groundbreaking impact on this field of research. In this study, the effects of multidentate oligoether additives on the structural characteristics of WCA-based electrolytes are examined. Integrating a linear oligoether of hexaglyme (G6) is found to be particularly effective at enhancing Mg plating/stripping performance, whereas the corresponding cyclic counterparts impart inferior performance. The combined electrochemical and spectroscopic analyses suggest that changes in the coordination environments of Mg^{2+} in solution with a specific amount of G6 are responsible for the enhanced interfacial charge-transfer kinetics. The results of this study will help guide the design of fully ethereal RMMB electrolytes compatible with highly reactive Mg metal-negative electrodes.

1. Introduction

Resource constraints require energy storage systems based on ubiquitous elements. Rechargeable Mg metal batteries (RMMBs) are a potential energy-storage technology that meets many of our current requirements.[1] The advantageous properties of Mg metal mean that the energy density of RMMBs could be comparable to that of lithium-ion batteries, but their material costs would be much lower.[2] Recent intensive research efforts to develop functional materials and advanced analytical techniques in conjunction with computational science have paved the way for a fundamental understanding of the working principles and bottleneck issues of RMMBs.[3–6] The results have contributed significantly to the development of electrode and electrolyte materials with improved electrochemical performance.[7–12]

Among various potential candidates, electrolytes incorporating a specific aluminate-based weakly coordinated anion (WCA), $[Al(HFIP)_4]^-$, with diglyme (G2) have exceptional compatibility with reversible Mg plating/stripping reactions.[13,14] The tentative optimum electrolyte, namely, 0.3–0.4 M $Mg[Al(HFIP)_4]_2$/G2 (M; mol dm^{-3}), demonstrated near-unity efficiency for Mg plating/stripping. However, its electrochemical performance with respect to cycle life and cycling efficiency is short of the target value, especially under practical experimental conditions. Specifically, the cycling efficiency is ≈98–99% at 1 mA cm^{-2} (Figure S1, Supporting Information), while the value reaches >99% over 250 cycles at 0.5 mA cm^{-2}.[13] Under relatively harsh experimental conditions, inferior cycling efficiency can be ascribed to side reactions during Mg plating/stripping. The introduction of functional artificial interfaces is a common strategy for mitigating undesired side reactions. A suitable Mg^{2+}-conductive interface has been achieved by rationally designed artificial interfaces, which effectively suppress side reactions while facilitate interfacial charge-transfer reaction simultaneously.[15–18] However, the construction of long-term stable artificial interfaces on metal electrodes remains challenging because of the successive morphological changes of the electrodes associated with repeated plating/stripping.[18] The associated mechanical stress induced by the inhomogeneous morphological evolution also deteriorates the interface, resulting in a limited lifespan.[4,19]

Making an electrolyte stable against Mg plating/stripping is one of the most straightforward approaches for overcoming interfacial issues. A common strategy for solvation sheath regulation was adopted in this study. One of the potential working principles behind the improved electrochemical performance achieved by solvation sheath regulation is the suppression of side reactions due to the elimination of associated anions in electrolyte solutions.[20,21] The strong electric field of divalent Mg^{2+} polarizes the electronic states of surrounding species (solvents and counter anions). This polarization induces collective shifts in the energy levels of the ionization potential and electron affinity, which makes the solvents and anions oxidatively stable but reductively unstable.[22] Certain electrolyte systems incorporating highly associative BH_4^- are not in the case due to its excellent reductive stability even in the association with divalent Mg^{2+}.[23,24] However, the salt association state in solutions is

T. Mandai
Functional Electrolyte Synthesis Team
Research Center for Energy and Environmental Materials (GREEN)
National Institute for Materials Science (NIMS)
1-1 Namiki, Tsukuba, Ibaraki 305-0044, Japan
E-mail: mandai.toshihiko@nims.go.jp

Supporting information for this article is available on the WWW under https://doi.org/10.1002/batt.202500348

Research Article
doi.org/10.1002/batt.202500348
Chemistry Europe
European Chemical Societies Publishing

critical for the systems incorporating species those reductive stabilities spanning the electrode potential of Mg, such as $[N(CF_3SO_2)_2]$ and $[Z(HFIP)_4]$ (Z = B or Al).[22] Although the association ability of WCAs is considerably weak, recent experimental studies have suggested the presence of associated species in electrolyte solutions, even when incorporating WCAs.[25] Such associated species are potentially susceptible to reduction, resulting in inferior efficiency. The introduction of electrophilic anion receptors such as $AlCl_3$ and $B(OCH_2CF_3)_3$ is a potential approach to facilitate salt dissociation.[26,27] The structural bulkiness of most WCAs, however, hinders the accommodation of anion receptors in their environments.[14] The integration of nonethereal solvating agents such as amines and phosphates also deteriorates or inactivates the electrochemical performance of representative WCA-based RMMB electrolytes.[22,28]

Cyclic oligoethers, such as crown ethers, are the most representative solvating (complexing) agents.[29] The addition of crown ethers to conventional $Mg[N(SO_2CF_3)_2]_2$-based ethereal electrolyte solutions enhances Mg plating/stripping efficiency.[30] Strong solvation by the crown ether, arising from multidentate characteristics, weakens unfavorable Mg^{2+}–anion interactions, thereby suppressing anion decomposition. It is believed that the same approach can be adopted for WCA-based systems because the partial association of WCAs in solutions is presumed to be the reason for their insufficient performance. In this study, multidentate oligoethers were used as ethereal solvating agents to achieve favorable WCA-based fully ethereal electrolytes. A systematic electrochemical and spectroscopic study of the oligoether structural characteristics revealed that the interfacial charge-transfer kinetics were enhanced by the integration of certain multidentate linear oligoethers into the WCA-based electrolyte because of the change in the coordination state of Mg^{2+} and the consequent relaxation of Mg^{2+} solvation by the main ethereal solvent.

2. Results and Discussion

The galvanostatic cycling profiles of the 0.3 M $Mg[Al(HFIP)_4]_2$/G2 electrolytes with and without 0.1 M oligoether additives are shown in **Figure 1**. The molecular structure formula of the additives is displayed in **Scheme 1**. In contrast to conventional RMMB electrolyte solutions, the efficacy of crown ether integration into WCA-based electrolytes is limited. The cycling efficiencies for Mg plating/stripping were improved slightly. However, cycle lives and polarization deteriorated compared with the control experiment using the base electrolyte, irrespective of the crown ether cavity size (*i.e.*, 2.0 Å for 15-crown-5 ether (15C5), while 2.9 Å for 18-crown-6 ether (18C6)).[29] The polarization curves in the initial cycles (Figure 1c) and the plot of overpotential at an areal capacity of 0.5 mAh cm^{-2} (Figure S2, Supporting Information) clearly indicate the negative effect of crown ether integration, especially in the case of 15C5. The size of the cavity and guest ions determines the binding affinity, and the cavity size of 15C5 matches well with Mg^{2+}.[29,31] This is one reason why remarkably large overpotentials are required for plating and stripping with 15C5. A similar result was reported for $Mg[N(CF_3SO_2)_2]_2$-based electrolytes, where the introduction of 15C5 resulted in no Mg plating activity.[30] In this study, 18C6 did not improve the Mg plating/stripping performance, which is inconsistent with

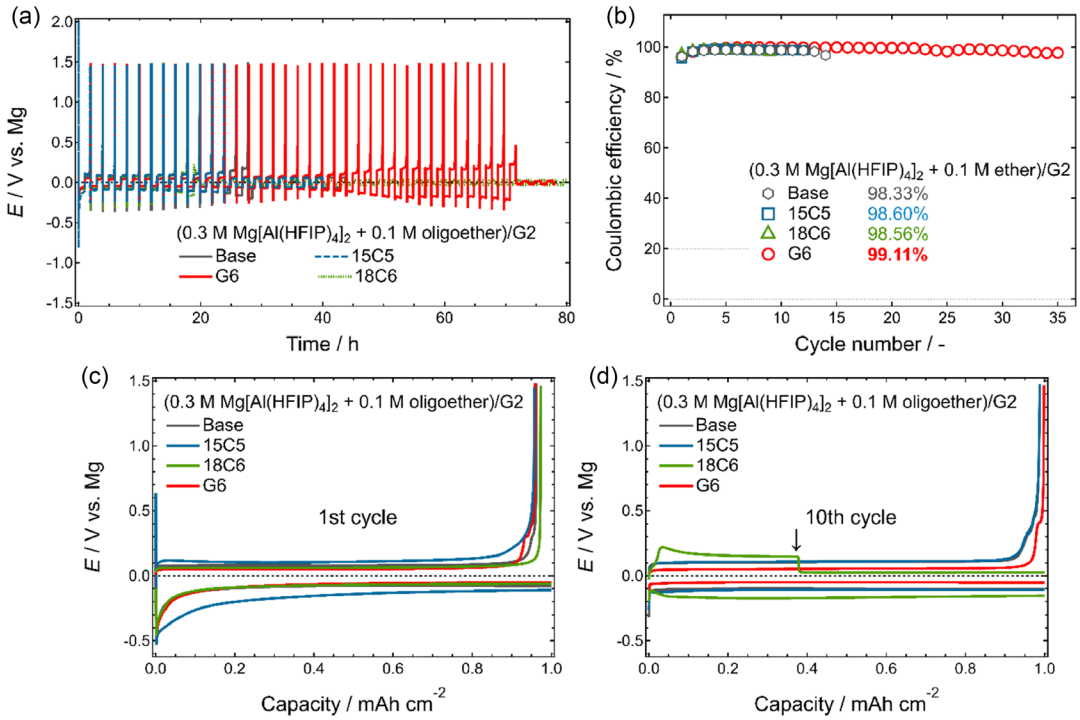

Figure 1. a) Galvanostatic cycling profile and b) corresponding Coulombic efficiency of asymmetric [Mg || Cu] cells using 0.3 M $Mg[Al(HFIP)_4]_2$/G2 with and without 0.1 M oligoether measured at 1 mA cm^{-2} and 30 °C. The legend in (b) indicates the Coulombic efficiency of each cell. Polarization curves during c) the 1st and d) 10th cycles. The arrow in (d) indicates the occurrence of a short-circuit.

Research Article
doi.org/10.1002/batt.202500348
Chemistry Europe
European Chemical Societies Publishing

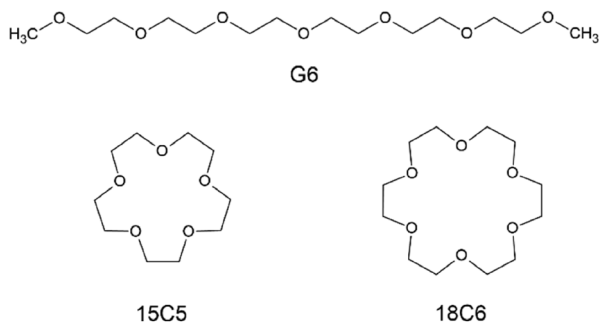

Scheme 1. Molecular structure formula of G6, 15C5, and 18C6.

previous studies. The polarization for Mg plating/stripping gradually increased with cycling, and the cycle life of the cell was reduced due to 18C6 integration compared with that of the control experiment. The larger polarization at the 10th plating/stripping cycle for 18C6 compared with that for 15C5 suggests the side reactions of the Mg metal with the electrolyte containing the 18C6.

In contrast to the above multidentate cyclic oligoethers, the integration of the linear oligoether G6 has a distinct impact on the Mg plating/stripping performance. The cycle life increased by almost three times without compromising the polarization characteristics. The electrolyte–Mg interface was stabilized by G6, as the polarization behavior during the 10th cycle was almost identical to that during the 1st cycle (Figure 1c,d). Comparative experiments using the shorter oligoethers G3 and G4 exhibited minor impacts on electrochemical characteristics (Figure S3, Supporting Information). In contrast, G6 imparted exceptional electrochemical characteristics. The Coulombic efficiency for the reversible Mg plating/stripping reached >99% over 30 cycles for the G6-integrated electrolyte, even at a relatively practical areal capacity of 1 mAh cm^{-2} (Figure 1b), while the values of the other systems were ≈98%. The integration of G6 was also particularly effective at improving the long-term cycling stability (Figure S4, Supporting Information).

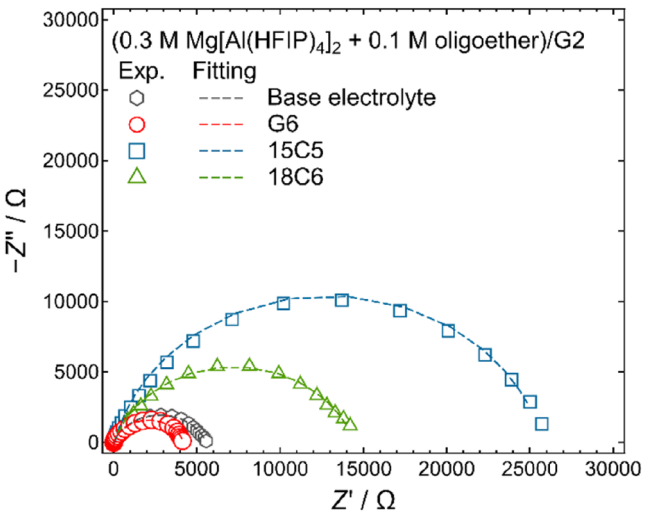

Figure 2. Nyquist plots of symmetric [Mg || Mg] cells using 0.3 M $Mg[Al(HFIP)_4]_2$/G2 with and without 0.1 M oligoether measured at 30 °C.

To provide in-depth insights into the interfacial behaviors of the different electrolytes, electrochemical impedance spectroscopy (EIS) was performed. Nyquist plots of the [Mg || Mg] symmetric cells were fitted using a typical equivalent circuit, and the fitting parameters are summarized in Table S1, Supporting Information. The oligoether additive has a dominant effect, especially on interfacial charge-transfer resistance (R_{CT}; **Figure 2** and Table S1, Supporting Information). The R_{CT} values increased significantly with the integration of cyclic oligoethers (crown ethers). An exceptionally large R_{CT} of the 15C5-based system demonstrated the strong binding of Mg^{2+} by 15C5 and hindered charge-transfer kinetics at the interface. The large R_{CT} was responsible for the remarkably large polarization observed during Mg plating/stripping using this electrolyte (Figure 1c). In stark contrast to cyclic oligoether-integrated systems, G6 integration facilitates interfacial charge-transfer kinetics. A similar positive effect was observed for the G4-integrated system, whereas G3 resulted in inferior interfacial behavior (Figure S5, Supporting Information). The preferential coordination number of Mg^{2+} in ethereal solutions is 5–6.[32] Systematic Raman spectroscopic analysis combined with X-ray crystallography and density functional theory calculations suggested that two orthogonally oriented solvent molecules wrapped the Mg^{2+} ions in the G2 and G3 solutions for stabilization.[33–35] However, a single, longer oligoether molecule can coordinate with several Mg^{2+} ions because of its conformational flexibility and multiple coordination sites. Such differences in coordination abilities can explain the different functions of G3 and longer glymes as agents for solvation sheath regulation.

The surface morphology of the cycled Mg electrodes was responsible for the improved cycle lifetimes of the G6-integrated electrolyte. In RMBs, uneven Mg plating/stripping reactions followed by the intrusion of three-dimensional (3D) Mg deposits into the porous separator are recognized as the main reasons for short circuits.[4,18,19,36] Scanning electron microscopy (SEM) images of Mg electrodes cycled in the base electrolyte show typical morphological evolution after stripping and plating reactions (**Figure 3**a). A number of pores generated during the electrochemical stripping processes were discernible, and bulk Mg crystals were unevenly deposited on the surface. In contrast, the surface appeared somewhat flat when Mg was cycled in an electrolyte containing G6 (Figure 3b). Microcrystalline deposits preferentially fill their pores, and a relatively small portion of Mg crystals is deposited adjacent to the former deposits. Eventually, the protrusion of 3D-deposited Mg is effectively mitigated by G6 integration, and this suppressed morphological evolution strongly contributes to the improved cycle life of Mg plating/stripping.

The Raman spectra of the electrolytes show the different solvation characteristics of the cyclic and linear oligoethers. The vibrational modes of the ethylene oxide units in oligoether molecules are sensitive to their solvation state.[37] While bulk oligoether solvents have broad peaks at ≈860–800 cm^{-1}, a distinct peak is discernible at ≈900–870 cm^{-1} upon complexation with metal ions, and this is the so-called ring breathing mode. The peak shift of the ring-breathing mode depends on the oligoether–metal ion interactions, shifting to higher wavenumbers with

Research Article
doi.org/10.1002/batt.202500348
Chemistry Europe
European Chemical Societies Publishing

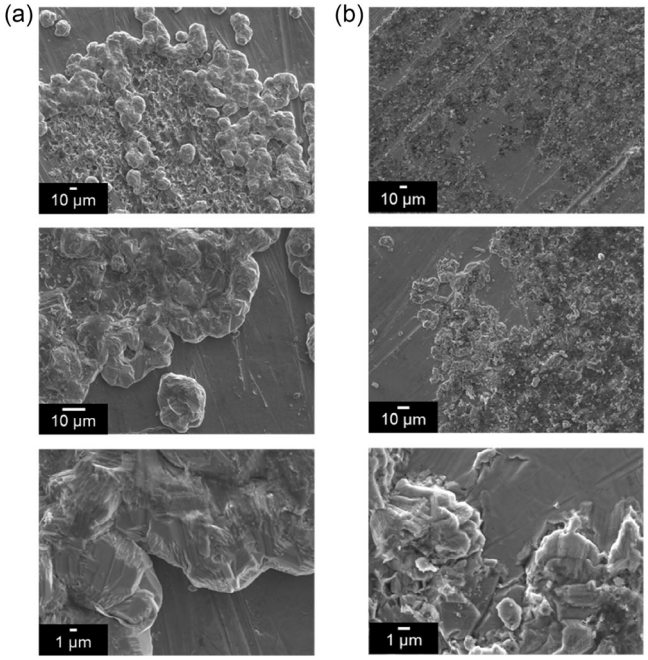

Figure 3. Outermost surface SEM images of the Mg electrodes after cycling. Cycled in the 0.3 M $Mg[Al(HFIP)_4]_2$/G2 electrolytes a) without and b) with 0.1 M G6.

increasing interactions. Indeed, monovalent Li^+–glyme complexes have the peak at ≈870 cm^{-1},[38–40] while the same peak appeared at ≈890 cm^{-1} for divalent Mg^{2+}–glyme complexes.[41–43]

The Raman spectra of the base electrolytes with and without oligoether additives are shown in **Figure 4**a. The spectrum of neat G2 was also used as a reference. The electrolytes exhibited characteristic spectral profiles. The distinct peak centered at 892 cm^{-1} observed in the base electrolyte is a fingerprint of the Mg^{2+}–G2 complex formation. The peak located at 765 cm^{-1} is assignable to the vibrational mode of the counter anion. Unfortunately, this band was less sensitive to the coordination state of the anion.[40] However, the addition of oligoethers to the base electrolyte affected the coordination state of Mg^{2+}, as evidenced by the change in the shift and shape of the corresponding peaks. The coordination state of Mg^{2+} drastically changed upon 15C5 integration because the peak intensity of the original Mg^{2+}–G2 complex decreased, and another peak appeared at higher wavenumbers. This observation indicates ligand exchange between G2 and 15C5 and two different coordination species, $[Mg(G2)_n]^{2+}$ and $[Mg(15C5)]^{2+}$, presented in the solution. As described above, the cavity size of 15C5 matches well with that of Mg^{2+}, which induces strong binding between Mg^{2+} and 15C5. However, for 18C6, the peak position of the fingerprint was almost identical to that of the base electrolyte, suggesting that G2 and 18C6 have comparable coordination ability. This may be explained by the size mismatch between Mg^{2+} and the cavity of 18C6 and the relatively rigid framework of 18C6.

Although the representative peak assignable to vibrational modes of anion is less sensitive to its coordination state, the transport properties clearly indicated improved dissociation of $Mg[Al(HFIP)_4]_2$ in G2 upon multidentate oligoether integration. As summarized in Table S2, Supporting Information, the ionic conductivity of the base electrolyte was greatly improved by the addition of the multidentate oligoethers irrespective of their structural characteristics. As the solution viscosity does not

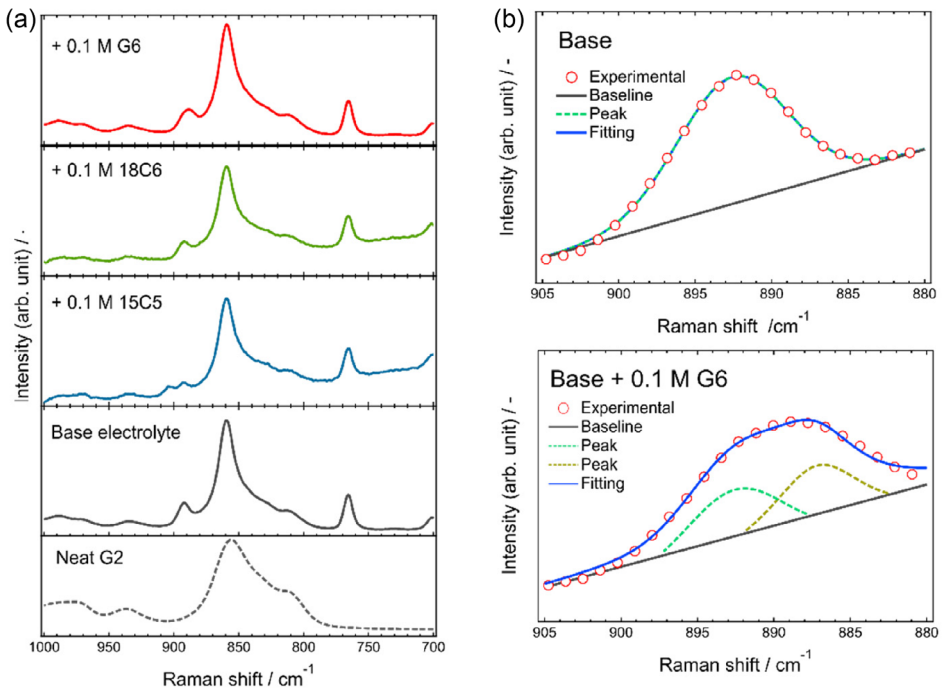

Figure 4. a) Raman spectra of 0.3 M $Mg[Al(HFIP)_4]_2$/G2 with and without 0.1 M oligoether at ambient temperature. The spectrum of a neat G2 solvent is included as a reference. The specific spectral range responsible for Mg^{2+}–ether coordination and the vibrational mode of the anion is depicted. b) Deconvolution of the fingerprint modes observed in 0.3 M $Mg[Al(HFIP)_4]_2$/G2 with and without 0.1 M G6.

Research Article
doi.org/10.1002/batt.202500348
Chemistry Europe
European Chemical Societies Publishing

change largely with and without the multidentate oligoethers, these oligoethers contributed to decrease associated Mg^{2+}–anion species. Among the studied oligoether, G6 integration imparted the highest conductivity. This observation suggests a different coordination manner of linear G6 against cyclic 15C5 and 18C6.

A different spectral feature was indeed observed for the electrolyte with linear G6. The peak position of the fingerprint of complexation shifted from 892 cm^{-1} for the base electrolyte to 888 cm^{-1} for the G6-integrated electrolyte, and the peak width was broadened. The spectral deconvolution provided clear evidence of change in coordination environment of Mg^{2+} in the G6-integrated electrolyte. The deconvolution results are shown in Figure 4b. The deconvolution and subsequent fitting of the fingerprint of the electrolytes with and without the G6 additive revealed the presence of two components, located at 892 and 887 cm^{-1}, in the former system. This change indicates relaxation of the Mg^{2+}–G2 interaction and an increase in the population of loosely bound Mg^{2+}-complexes in the solution. Because the desolvation process at the Mg–electrolyte interface is the rate-determining step for Mg plating,[44] the weakened interaction facilitates charge-transfer kinetics at the interface. This is also effective in suppressing undesired side reactions, resulting in enhanced Mg plating/stripping performance with G6 integration. Revealing the detailed mechanism of the coordination change by G6 is beyond the scope of this study and will be investigated in future work using structural analysis combined with theoretical calculations.

To clarify the composition–performance relationship in the presented system, the effect of the G6 concentration was evaluated. The G6 concentration has a dominant impact on electrochemical performance (**Figure 5**). The optimal composition for Mg plating/stripping should be a base electrolyte with 0.1 M G6; however, the performance decreases with increasing G6 concentrations. The cycle lives are almost the same among the electrolytes, with the exception of 0.1 M G6. However, the Coulombic efficiency of Mg plating/stripping degraded with the increasing G6 concentration (Figure 5b). The considerably poor electrochemical performance of the electrolyte comprising the same conductive salt and G6, 0.3 M $Mg[Al(HFIP)_4]_2$/G6, compared to that of the base electrolyte, implies insufficient compatibility of excess G6 with Mg plating/stripping reactions (Figure S6, Supporting Information). In addition to the cycle life and cycling efficiency, the polarization behavior of Mg plating/stripping is also dependent on the concentration of G6. A substantially large overpotential was observed for the electrolytes containing certain amounts of G6. However, the plots of the stable plating/stripping polarization, e.g., the voltage at an areal capacity of 0.5 mAh cm^{-2}, as a function of G6 concentration, represented the concave/convex-type profiles for plating/stripping, respectively (Figure S7, Supporting Information). The interfacial resistance exhibited a similar trend (Figure S8, Supporting Information). These observations strongly suggest changes in the coordination state of Mg^{2+} at specific electrolyte compositions.

Assuming that the associative nature of $[Al(HFIP)_4]^-$ is comparable to that of $[B(HFIP)_4]^-$, ≈20% of the anion should be

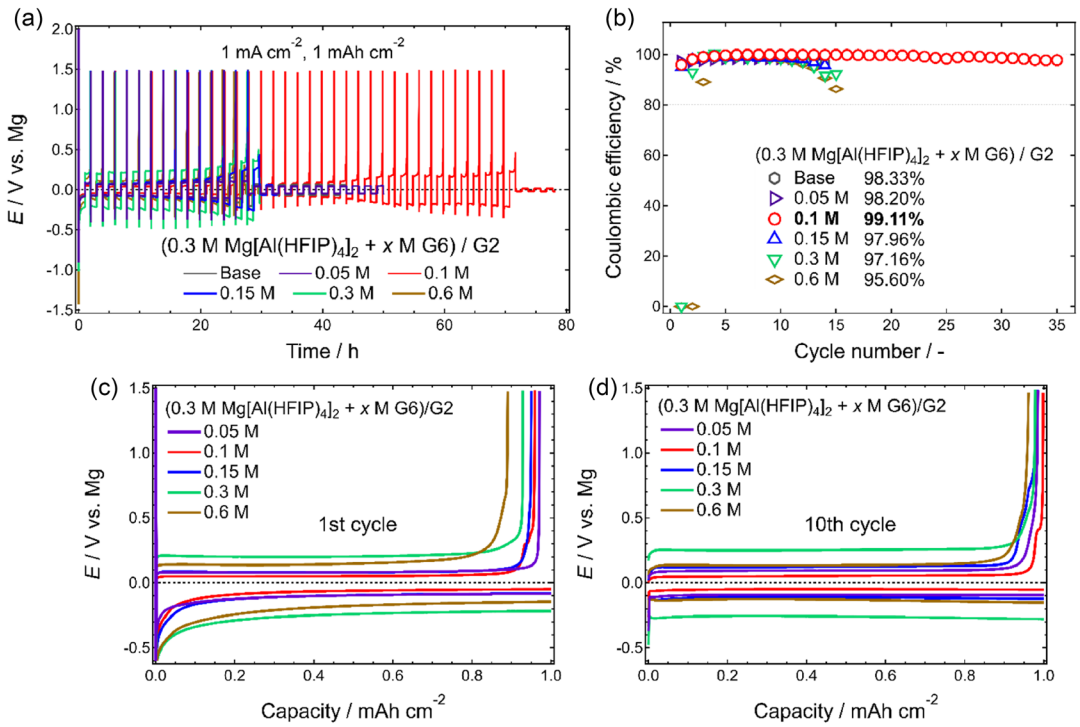

Figure 5. a) Galvanostatic cycling profiles and b) corresponding Coulombic efficiencies of asymmetric [Mg || Cu] cells using (0.3 M $Mg[Al(HFIP)_4]_2$ + *x* M G6)/G2 electrolytes measured at 1 mA cm^{-2} and 30 °C. The legend in (b) represents the average Coulombic efficiency of each cell. Polarization curves for c) the 1st and d) 10th cycles.

loosely bound to Mg^{2+} in the solution, according to the preceding work.[23] Based on the composition of the base electrolyte, the addition of a certain amount of G6 with greater solvation ability than G2 can effectively facilitate the dissociation of the remaining associated species. Elimination of associated species would enhance the electrochemical Mg plating/stripping performance. However, an excess of G6 causes a coordination exchange between G2 and G6, which leads to the formation of a dominant amount of $[Mg(G6)]^{2+}$. The desolvation energy of $[Mg(G6)]^{2+}$ is definitely larger than that of $[Mg(G2)_n]^{2+}$ because of its well-known chelating effect. This is partly why large polarization is necessary for Mg plating/stripping in an electrolyte containing 0.3 M G6. However, the further addition of more G6 caused further changes in the coordination environment of Mg^{2+} but in a different manner because of the conformational flexibility and multidentate nature of G6. Several G6 molecules participate in the coordination of single Mg^{2+}, and this can reduce the binding power of each G6 molecule against Mg^{2+}. The post-analysis on the Raman spectra also supports this hypothesis. The spectral deconvolution suggested the formation of three different solvates depending on the G6 concentration. The deconvolution results of the selected spectra and fraction of each deconvoluted peak are summarized in Figure S9, Supporting Information. As shown in Figure 4b and S9, Supporting Information, while the base G2-based electrolyte has a single peak located at 892 cm^{-1}, the addition of a small amount of G6 resulted in the formation of the G6-solvate, which was observed at 887 cm^{-1} in their spectra, possibly accompanied with the dissociation of the remaining associated species. At the G6 concentration of 0.3 M, all solvates presented in the solution should be replaced into $[Mg(G6)]^{2+}$ due to the strong chelating effect of G6, and the single peak located at 887 cm^{-1} has indeed been found in the corresponding spectrum. Notably, excess G6 resulted in the distinct peak evolution at 893 cm^{-1} (Figure S9, Supporting Information). This new peak can be assigned to the above different solvate species. Crystallographic studies on binary mixtures of Li salt and oligoethers have indeed identified the different solvate formation depending on the ratio of salt and oligoethers: isolated column-like and polymeric chain-like structures.[45] Owing to the structural similarity, a similar coordination capability is expected for G6. Although further detailed structural analysis is needed to identify the exact coordination environment of Mg^{2+} in our system, such a change in the coordination environment due to the ratio between Mg^{2+} and G6 may result in a convex/concave-type composition–polarization relationship.

Finally, the compatibility of the developed electrolyte with representative positive electrodes is assessed. Discharge–charge cycling performance of the [Mg || Mo_6S_8] cells using the base and optimal electrolytes is shown in **Figure 6**. The deliverable capacities were comparable, irrespective of the electrolyte formulation. This result is understandable because the polarization characteristics of these electrolytes were almost identical (Figure S7, Supporting Information). In contrast, the reproducibility of the battery cycling results improved remarkably with the optimal electrolyte. The profiles of the two independent measurements overlapped well, particularly for charging, whereas those obtained using the base electrolyte exhibited inferior reproducibility. Although many independent and mutually correlated factors contribute to the conclusive battery cycling performance, the improved interfacial characteristics induced by G6 integration may minimize the negative contributions, which would impart a fluctuating performance, and eventually lead to greater experimental reproducibility.

3. Conclusion

This study investigated the effects of oligoether additives on the electrochemical Mg plating/stripping performance of representative WCA-based electrolytes. A systematic survey of the molecular structure of oligoethers revealed that the introduction of cyclic oligoethers into the base electrolyte negatively affected the electrochemical performance, although its effectiveness has been reported for other systems incorporating associative anions. In contrast, the electrochemical performance was remarkably improved after integrating a specific linear oligoether of G6. EIS combined with Raman spectroscopy analysis indicated that the interfacial charge-transfer kinetics were enhanced by G6 integration owing to changes in the coordination state of Mg^{2+} in the electrolytes and consequent relaxation of the Mg^{2+}–G2 interaction. The flexible chain structure and the large number of coordination sites in a single G6 molecule are responsible for such

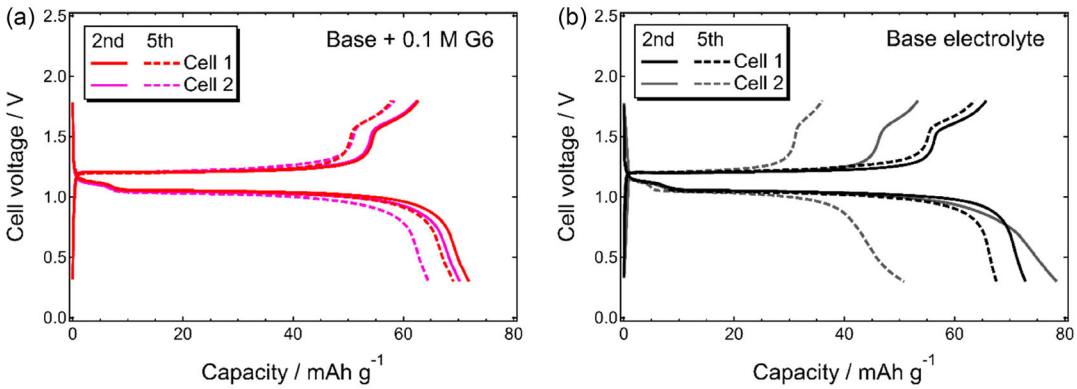

Figure 6. Discharge–charge cycling profiles of [Mg || Mo_6S_8] cells using a) optimal and b) base electrolytes.

favorable coordination environments. The optimum G6-integrated fully ethereal WCA electrolyte allowed stable Mg plating/stripping cycling with improved Coulombic efficiency. This electrolyte also improved the reproducibility of the battery cycling performance.

The development of prospective electrolyte materials that satisfy various requirements for practical RMMB materialization has been a long-standing challenge in this field of research. Regulation of the solvation sheath by solvating nonethereal solvents is an emerging concept for improving the overall performance of RMMB electrolytes. However, the selective compatibility of Mg with organic solvents and the resulting large polarization for Mg plating/stripping may limit the application of these nonethereal solvents in practical batteries.[7] This work provides another pathway for designing rational electrolyte materials based on fully ethereal solvents that are ultimately compatible with reactive Mg metal-negative electrodes.

4. Experimental Section

Materials

A conductive salt consisting of the representative WCA, $Mg[Al(HFIP)_4]_2$, was synthesized according to a previously reported procedure with a slight modification to the isolation step.[13] The crude product was purified by washing with anhydrous diethyl ether (FUJIFILM Wako Chemicals) until the solution phase became colorless, followed by vacuum drying at 45 °C for 2 h, yielding microcrystalline colorless products. The chemical structures and compositions were determined by ^1H and ^{19}F NMR spectroscopy, and the spectra were identical to those previously reported. Anhydrous G2 and G3 were obtained from Kanto Chemical Co., Inc., and used as received. G4 was purchased from Kishida Chemical Co., Ltd., and G6 was obtained from the NARD Institute, Ltd. Both G4 and G6 were dehydrated over 4 A molecular sieves prior to use. We obtained 15-crown-5 ether (15C5) and 18-crown-6 ether (18C6) from Tokyo Chemical Industry Co., Ltd., and they were used without further purification. The electrolyte solutions were prepared by mixing predetermined amounts of $Mg[Al(HFIP)_4]_2$ and a specific oligoether in G2, followed by vigorous stirring at 30 °C overnight in an Ar-filled glovebox (<1 ppm H_2O and O_2). For electrolytes containing 15C5 or 18C6, the resulting solutions were dried over 4 A molecular sieves for several days. The water content of the prepared electrolytes was determined to be 50–100 ppm using Karl Fischer titration. $Cu_2Mo_6S_8$, a precursor of the positive electrode active material, was purchased from Kojundo Chemical Laboratory Co., Ltd., and oxidized to obtain Mo_6S_8 powder following a standard oxidation protocol.[46]

Electrochemical Measurements

Galvanostatic Mg plating/stripping measurements were conducted on asymmetric and symmetric two-electrode cells. Asymmetric cells were fabricated using Cu foil and Mg metal. To remove native oxide films, Cu foil was soaked in a 0.1 M HCl aqueous solution for 1 h, rinsed with deionized water, ethanol, and acetone, and then dried under vacuum at 80 °C overnight. For the Mg (Rikazai; 99.94%, $t = 0.04$ mm) electrodes, the surface was polished mechanically with sandpaper, washed several times with anhydrous tetrahydrofuran (THF), and dried under vacuum at ambient temperature for 1 h, irrespective of the cell assemblies. The pretreatment of the Mg electrodes and all cell assemblies was performed in an Ar-filled glovebox. Mo_6S_8 composite electrodes were fabricated according to a previously reported procedure.[18] The average loading of Mo_6S_8 was fixed at ≈2 mg cm^{-2}. A glass fiber separator (GF/A, $t = 0.260$ mm) was used as the standard separator for all electrochemical measurements, unless otherwise specified. Galvanostatic and discharge–charge measurements were conducted using an automatic charge–discharge instrument (HJ0610SD8C, Hokuto-Denko Co., Ltd.). For the galvanostatic Mg plating/stripping cycling measurements, a fixed current density of 1 mA cm^{-2} was applied. The battery cycling test was conducted at 0.3–1.8 V and 30 °C with a current density of 12.2 mA g^{-1}, based on the mass of Mo_6S_8. The EIS spectra of the [Mg || Mg] symmetric cells were acquired using the complex impedance method with an impedance analyzer (VMP3, Biologic). The current frequency of the cells was scanned from 1 to 50 mHz with a sinusoidal alternating voltage amplitude of a 10 mV root mean square.

Characterization

The surfaces of the cycled Mg electrodes were observed using SEM (JSM-7800 F, JEOL). The Mg electrodes retrieved from the cycled cells were washed with anhydrous THF to remove the residual electrolyte, dried under high vacuum at ambient temperature, placed in an airtight chamber, and transferred for SEM analysis without air exposure.

The coordination states of Mg^{2+} in solution were evaluated using Raman spectroscopy. The spectra were collected using a laser Raman spectrometer (NRS-4500, JASCO) equipped with a 785-nm laser at a resolution of 1 cm^{-1}. The sample solutions were hermetically sealed in quartz glass tubes in an Ar-filled glovebox and were subjected to spectrometry without any exposure to moisture. The acquired spectra were calibrated using a Si standard. The spectral deconvolution was carried out by the Gaussian–Lorentzian function.

The ionic conductivities of a series of electrolyte solutions were measured using the complex impedance method with an impedance analyzer (VMP3, Biologic). A commercial cell equipped with two platinized platinum electrodes (CT-57101B, TOA DKK Corporation) was used for the measurements. The cell was placed in a temperature-controlled chamber and held at 30 °C for 1 h to equilibrate the temperature prior to the measurements. The viscosities were measured at 30 °C using a kinematic viscometer (SVM3001, Anton Paar GmbH). All of the standard deviations in the experimental values were within ±3% of the average.

Acknowledgements

This work was supported in part by the GteX Program (grant number JPMJGX23S1) and the NEXT Center of Innovation Program (grant number JPMJPF2016) of the Japan Science and Technology Agency. The authors acknowledge Ms. Watanabe and Ms. Oshida for their support in the electrochemical measurements and SEM observations. SEM images were acquired at the Battery-PF facilities of the National Institute for Materials Science.

Conflict of Interest

The author declares no conflict of interest.

Data Availability Statement

The data that support the findings of this study are available from the corresponding author upon reasonable request.

Keywords: electrolytes · ether · magnesium batteries · multidentate · salvation

[1] J. A. Blázquez, R. R. Maça, O. Leonet, E. Azaceta, A. Mukherjee, Z. Zhao-Karger, Z. Li, A. Kovalevsky, A. Fernandez-Barquín, A. R. Mainar, P. Jankowski, L. Rademacher, S. Dey, S. E. Dutton, C. P. Grey, J. Drews, J. Häcker, T. Danner, A. Latz, D. Sotta, M. R. Palacin, J.-F. Martin, J. M. G. Lastra, M. Fichtner, S. Kundu, A. Kraytsberg, Y. Ein-Eli, M. Noked, D. Aurbach, *Energy Environ. Sci.* **2023**, *16*, 1964.
[2] I. D. Johnson, B. J. Ingram, J. Cabana, *ACS Energy Lett.* **2021**, *6*, 1892.
[3] S. Okamoto, T. Ichitsubo, T. Kawaguchi, Y. Kumagai, F. Oba, S. Yagi, K. Shimokawa, N. Goto, T. Doi, E. Matsubara, *Adv. Sci.* **2015**, *2*, 1500072.
[4] M. J. Park, H. Y. Asl, A. Manthiram, *ACS Energy Lett.* **2020**, *5*, 2367.
[5] N. N. Rajput, X. Qu, N. Sa, A. K. Burrell, K. A. Persson, *J. Am. Chem. Soc.* **2015**, *137*, 3411.
[6] X. Liu, A. Du, Z. Guo, C. Wang, X. Zhou, J. Zhao, F. Sun, S. Dong, G. Cui, *Adv. Mater.* **2022**, *34*, 2201886.
[7] K. Shimokawa, T. Atsumi, N. L. Okamoto, T. Kawaguchi, S. Imashuku, K. Wagatsuma, M. Nakayama, K. Kanamura, T. Ichitsubo, *Adv. Mater.* **2021**, *33*, 2007539.
[8] Y. Xiu, A. Mauri, S. Dinda, Y. Pramudya, Z. Ding, T. Diemant, A. Sarkar, L. Wang, Z. Li, W. Wenzel, M. Fichtner, Z. Zhao-Karger, *Angew. Chem., Int. Ed.* **2023**, *62*, e202212339.
[9] J. T. Herb, C. A. Nist-Lund, C. B. Arnold, *ACS Energy Lett.* **2016**, *1*, 1227.
[10] Z. Zhao-Karger, M. E. G. Bardaji, O. Fuhr, M. Fichtner, *J. Mater. Chem. A* **2017**, *5*, 10815.
[11] T. Mandai, H. Somekawa, *Chem. Commun.* **2020**, *56*, 12122.
[12] Z. Song, Z. Zhang, A. Du, S. Dong, G. Li, G. Cui, *Adv. Mater.* **2021**, *33*, 2100224.
[13] T. Mandai, Y. Youn, Y. Tateyama, *Mater. Adv.* **2021**, *2*, 6283.
[14] T. Pavčnik, M. Lozinšek, K. Pirnat, A. Vizintin, T. Mandai, D. Aurbach, R. Dominko, J. Bitenc, *ACS Appl. Mater. Interfaces* **2022**, *13*, 26766.
[15] K. Tang, A. Du, S. Dong, Z. Cui, X. Liu, C. Lu, J. Zhao, X. Zhou, G. Cui, *Adv. Mater.* **2020**, *32*, 1904987.
[16] Z. Meng, Z. Li, L. Wang, T. Diemant, D. Bosubabu, Y. Tang, R. Berthelot, Z. Zhao-Karger, M. Fichtner, *ACS Appl. Mater. Interfaces* **2021**, *13*, 37044.
[17] Z. Li, T. Diemant, Z. Meng, Y. Xiu, A. Reupert, L. Wang, M. Fichtner, Z. Zhao-Karger, *ACS Appl. Mater. Interfaces* **2021**, *13*, 33123.
[18] T. Mandai, U. Tanaka, M. Watanabe, *Energy Storage Mater.* **2024**, *67*, 103302.
[19] J. Eaves-Rathert, K. Moyer, M. Zohair, C. L. Pint, *Joule* **2020**, *4*, 1324.
[20] S. Hou, X. Ji, K. Gaskell, P. Wang, L. Wang, J. Xu, R. Sun, O. Borodin, C. Wang, *Science* **2021**, *374*, 172.
[21] M. Wang, W. Sun, K. Zhang, Z. Zhang, A. Du, S. Dong, J. Zhang, J. Liu, X. Chen, Z. Zhou, F. Li, Z. Li, G. Li, G. Cui, *Energy Environ. Sci.* **2024**, *17*, 630.
[22] T. Mandai, M. Yao, K. Sodeyama, A. Kagatsume, Y. Tateyama, H. Imai, *J. Phys. Chem. C* **2023**, *127*, 10419.
[23] R. Mohtadi, M. Matsui, T. S. Arthur, S.-J. Hwang, *Angew. Chem., Int. Ed.* **2012**, *51*, 9780.
[24] F. Tuerxun, K. Yamamoto, M. Hattori, T. Mandai, K. Nakanishi, A. Choudhary, Y. Tateyama, K. Sodeyama, A. Nakao, T. Uchiyama, M. Matsui, K. Tsuruta, Y. Tamenori, K. Kanamura, Y. Uchimoto, *ACS Appl. Mater. Interfaces* **2020**, *12*, 25775.
[25] J. Bitenc, K. Pirnat, O. Lužanin, R. Dominko, *Chem. Mater.* **2024**, *36*, 1025.
[26] H. S. Kim, T. S. Arthur, G. D. Allred, J. Zajicek, J. G. Newman, A. E. Rodnyansky, A. G. Oliver, C. Boggess, J. Muldoon, *Nat. Commun.* **2011**, *2*, 427.
[27] C. Chen, J. Chen, S. Tan, X. Huang, Y. Du, B. Shang, B. Qu, G. Huang, X. Zhou, J. Wang, L. Li, F. Pan, *Energy Storage Mater.* **2023**, *59*, 102792.
[28] T. Mandai, *ChemSusChem* **2025**, in press, https://doi.org/10.1002/cssc.202500418.
[29] C. J. Pedersen, H. K. Frensdorff, *Angew. Chem., Int. Ed.* **1972**, *11*, 16.
[30] I. Weber, J. Ingenmey, J. Schnaidt, B. Kirchner, R. J. Behm, *ChemElectroChem* **2021**, *8*, 390.
[31] R. D. Shannon, *Acta Cryst.* **1976**, *A32*, 751.
[32] S. Tsuzuki, T. Mandai, S. Suzuki, W. Shinoda, T. Nakamura, T. Morishita, K. Ueno, S. Seki, Y. Umebayashi, K. Dokko, M. Watanabe, *Phys. Chem. Chem. Phys.* **2017**, *19*, 18262.
[33] T. Kimura, K. Fujii, Y. Sato, M. Morita, N. Yoshimoto, *J. Phys. Chem. C* **2015**, *119*, 18911.
[34] K. Fujii, M. Sogawa, N. Yoshimoto, M. Morita, *J. Phys. Chem. B* **2018**, *122*, 8712.
[35] O. Tutusaus, R. Mohtadi, T. S. Arthur, F. Mizuno, E. G. Nelson, Y. V. Sevryugina, *Angew. Chem., Int. Ed.* **2015**, *54*, 7900.
[36] T. Mandai, *ACS Appl. Mater. Interfaces* **2020**, *12*, 39135.
[37] D. Brouillette, D. E. Irish, N. J. Taylor, G. Perron, M. Odziemkowski, J. E. Desnoyers, *Phys. Chem. Chem. Phys.* **2002**, *4*, 6063.
[38] K. Ueno, R. Tatara, S. Tsuzuki, S. Saito, H. Doi, K. Yoshida, T. Mandai, M. Matsugami, Y. Umebayashi, K. Dokko, M. Watanabe, *Phys. Chem. Chem. Phys.* **2015**, *17*, 8248.
[39] T. Mandai, K. Yoshida, S. Tsuzuki, R. Nozawa, H. Masu, K. Ueno, K. Dokko, M. Watanabe, *J. Phys. Chem. C* **2015**, *119*, 1523.
[40] T. Mandai, H. Naya, H. Masu, *J. Phys. Chem. C* **2023**, *127*, 7987.
[41] S. Terada, T. Mandai, S. Suzuki, S. Tsuzuki, K. Watanabe, Y. Kamei, K. Ueno, K. Dokko, M. Watanabe, *J. Phys. Chem. C* **2016**, *120*, 1353.
[42] K. Hashimoto, S. Suzuki, M. L. Thomas, T. Mandai, S. Tsuzuki, K. Dokko, M. Watanabe, *Phys. Chem. Chem. Phys.* **2018**, *20*, 7998.
[43] T. Mandai, K. Tatesaka, K. Soh, H. Masu, A. Choudhary, Y. Tateyama, R. Ise, H. Imai, T. Takeguchi, K. Kanamura, *Phys. Chem. Chem. Phys.* **2019**, *21*, 12100.
[44] J. Drews, P. Jankowski, J. Häcker, Z. Li, T. Danner, J. M. G. Lastra, T. Vegge, N. Wagner, K. A. Friedrich, Z. Zhao-Karger, M. Fichtner, A. Latz, *ChemSusChem* **2021**, *14*, 4820.
[45] C. Zhang, S. J. Lilley, D. Ainsworth, E. Staunton, Y. G. Andreev, A. M. Z. Slawin, P. G. Bruce, *Chem. Mater.* **2008**, *20*, 4039.
[46] M. D. Levi, E. Lancry, H. Gizbar, Z. Lu, E. Levi, Y. Gofer, D. Aurbach, *J. Electrochem. Soc.* **2004**, *151*, A1044.

Manuscript received: May 6, 2025
Revised manuscript received: June 9, 2025
Version of record online: September 4, 2025